

## By using Doctor Blade Method, Lithium and Magnesium Co-Doped with Nickel Oxide Thin Film as Charge Transport Layer for Inorganic Perovskite Solar Cell

Abdul Rehman<sup>1\*</sup>, Shahzad Naseem<sup>2</sup>

<sup>1</sup>Centre of Excellence in Solid State Physics, University of the Punjab Quaid-i-Azam Campus, Lahore, 54000, Punjab, Pakistan

<sup>2</sup>Nano Science and Technology Department, National Centre For Physics, Quaid-i-Azam University, Islamabad, 44000, Pakistan

**Corresponding Author's email:** abdulr71682@gmail.com

### ABSTRACT

The organic materials for hole transport layer HTL such as PEDOT: PSS and Spiro-OMeTAD are poor electron blockers, more expensive, unstable, and large charge recombination materials. The inorganic material such as nickel oxide and copper oxide thin film for hole transport layer HTL was used to enhance the fill factor FF, power conversion efficiency PCE and stability of the hole transport layer for inorganic perovskite solar cell. Lithium and Magnesium co-doped with nickel oxide nanoparticles deposited on indium doped tin oxide ITO glass then deposited the cesium lead iodide bromide layer by using doctor blade method then characterize this thin film for confirmed the properties of the materials. The crystal structure of nickel oxide was measured from XRD and all the peaks were matched with JCPDS cards. The average crystalline size was 24 nm has cubic in shape. For optical properties and bandgap measured, using UV visible and DRS confirmed the strong absorbance near to the visible range, and bandgap decreased from 3.7 to 3.4 eV by adding doping. After the deposition of the inorganic perovskite layer, the bandgap decreased from 3.09 eV to 2.56 eV. RBS confirmed the chemical composition, impurity, and thickness of the thin film. The IV curve measurement showed the 4.3 % efficiency of the pure nickel oxide thin film, by adding the doping of lithium and magnesium in nickel oxide thin film showed the 7.65 % efficiency with the 83 % fill factor FF.

**Keywords:** Organic-inorganic perovskite, Solar cell, Doctor blade, Co-precipitation, Power conversion efficiency, Fill factor, Doped.

### Article History

Received: 30<sup>th</sup> December, 2021

Accepted: 23<sup>rd</sup> February, 2022

Published: 26<sup>th</sup> February, 2022

### Creative Commons License



NUST Journal of Natural Sciences (NJNS) is licensed under a Creative Commons Attribution 4.0 International License

### INTRODUCTION

A monocrystalline silicon-based solar cell is the major kind of commercial solar cell

(Ranabhat et al.,2016). The main problem with the silicon-based solar cell is the very high cost due to the high energy consumption and the high price of the procedures desirable to refine the physical to make the solar cell

ideals. To reduce these drawbacks, there are many technologies are being observed. Since 2009, organic and inorganic hybrid Perovskite solar cells (PSCs) are a comparative much stranger comparative all the previous solar cells with the power conversion efficiencies of 3.8% to 24% (Ranabhat et al., 2016). The progress of this type of solar cell is achieved only eleven years with the comparable of silicon base solar cell have efficiency which was achieved in fifty years due to it has a large charge diffusion lengths and high light absorption coefficient (Ranabhat et al., 2016). To improve the efficiency and increase the stability for this type of solar cell replacing organic components with inorganic components is the best solution to the stability issue (Ranabhat et al., 2016; Liu, et al., 2018).

Recently, improvement in the composition of perovskite shown to tolerate more achievements of device stability, XR, as HC-(NH<sub>2</sub>)<sub>2</sub> and CH<sub>3</sub>NH<sub>3</sub> were substituted by rubidium, cesium, or guanidinium. We can increase the stability of perovskite by replacing the bromide, thiocyanate, and chloride instead of iodine. There are different methods available for the deposition of perovskite with thermal evaporation two-step deposition and anti-solvent dripping which affect the morphology of the perovskite layers, By increasing the crystallinity, its efficiency increased by 22% with the approaching the commercial solar cells (Ranabhat et al., 2016). Increasing the lifetime of PSCs is the main challenge, there are many problems such as the upscaling and toxic lead used.

There many organic materials are available for hole transport layers such as PEDOT: PSS, salts of lithium, Spiro-OMeTAD, and PTAA has a lot of drawbacks and faces many problems, such as irregular quality from distributors, weak electron blocker, hygroscopic in nature, air and moisture stabilities of these devices has serious issue (Ranabhat et al., 2016). PEDOT: PSS films reduce the performance of the device. Mostly used Spiro-OMeTAD as HTL in PSCs which

is complicated and more expensive (Ranabhat et al., 2016).

The inorganic p-type materials as metal oxide can give carrier mobility, large stability, low cost, and easy alignment of the bandgap (Ranabhat et al., 2016). For making the highest photo and thermal stable PSCs there are different types of metal oxide or p-type materials are available as used for hole transport layers such as CuO, Cu<sub>2</sub>O, MoO<sub>3</sub>, WO<sub>3</sub>, V<sub>2</sub>O<sub>5</sub>, and NiO<sub>x</sub>. The mobility of holes is about 10<sup>5</sup>–10<sup>3</sup> m<sup>2</sup>/V s, high stability of the air, and open-circuit voltage V<sub>oc</sub> is larger than the PEDOT: PSS. Nickel Oxide has become a favorable HTL for PSCs with simple preparation methods and has an efficiency of up to 10% (Ranabhat et al., 2016). Open circuit voltage V<sub>oc</sub> and power conversion efficiency PCE of metal oxide thin film higher than PEDOT: PSS (Liu et al., 2018). NiO has many advantages which consist of good electron-blocking and better conductivity. Synthesis of doped NiO by Solution based is very easy and its PCE can enhance the conductivity (Liu et al., 2018). In recent, many reported of inorganic perovskite structure devices with the Spiro-OMeTAD as HTL (Duan et al., 2018; Sanchez et al., 2018; Sveinbjörnsson et al., 2018; Liang et al., 2017; Wang et al., 2018; Liao et al., 2018; Murugadoss et al., 2019; Zhang et al., 2019; Lei et al., 2018; Beal et al., 2016; Frolova et al., 2016; Zhang et al., 2018; Chen et al., 2019; Mali et al., 2018; He et al., 2018; Sun et al., 2018; Zhang et al., 2008; Irwin et al., 2008).

Inorganic perovskite structure devices with metal oxide thin film are also reported, (Qin et al., 2017; Irwin et al., 2008; Zhang et al., 2016; Fu et al., 2019; Chen et al., 2017; Sun et al., 2018; Ouyang et al., 2019; Xiang et al., 2018; Mali et al., 2018).

## MATERIALS AND METHODS

In the experimental techniques, we produced the nanomaterial and nanostructure materials

of nickel oxide, Lithium doped nickel oxide, magnesium-doped nickel oxide, and co-doped lithium and magnesium in nickel oxide by using the co-precipitation method. After the achieved of nano powdered was changed into thin-film by deposited on a glass substrate with the doctor blade method to study the chemical, optical, mechanical, crystal, and electrical properties.

### Preparation of Nickel Oxide by Co-Precipitation Method

First of all, take the nickel salt of metal as  $\text{NiCl}_2$  is dissolved in a solvent as deionized water, then the precipitating agent as NaOH was added dropwise to maintain the pH.  $\text{Ni}(\text{OH})_2$  was obtained in the form of precipitating and has much unnecessary material. To reduce this material, filtrate it, then washed by deionized water. After that, this solution was dried in an oven at  $120^\circ\text{C}$ . For obtaining the metal oxide, annealed it at a furnace in the presence of oxygen at  $450^\circ\text{C}$ .

For doping of the material, add 5% of lithium and 5% of magnesium into the salt of nickel separately and repeat the same procedure as the undoped material. For co-doped, both lithium and magnesium were added combined into the salt of nickel also repeating the same procedure as undoped material (Thambidurai et al., 2020).

### Making Thin Film from Nanoparticles Powder

First of all, take the 1g of Nickel Oxide powder and added with 1ml of Ethanol, and make the solution into a blood testing tube. Sonicate this solution for 90 min at room temperature. Added a few drops of acetic acid to make the paste. When the solution is dissolved, it deposits on a glass substrate.

### Preparation of Inorganic Perovskite Layer by Doctor Blade Method

The doctor blade process is very easy and cheap. For the preparation of the perovskite layer, take the cesium iodide, lead bromide and lead iodide are in equal amounts. All the chemicals are measured and added into the small vials with a few drops of Dimethyl sulfoxide DMSO and Dimethyl Formamide DMF are added to make the solution, stirred it for half hours when the solution is dispersed and soluble then stop the stirring. In the end, investigated all the electrical, chemical, and optical properties of all these dopant solutions (Pei et al., 2020).

## RESULT AND DISCUSSION

### XRD Data Analysis

XRD analysis confirms the phase of the synthesized Nickel Oxide nanoparticles. After the calcination at  $450^\circ\text{C}$ , the crystalline phase matches the peaks from X-pert software. It was observed that NiO peaks are cubic structures and the peaks match with JCPDS card number ICSD 00-073-1523. At the crystalline phase all diffraction peaks at  $37.26^\circ$ ,  $43.3^\circ$ ,  $62.9^\circ$ ,  $75.43^\circ$  and  $79.43^\circ$  are planes (111), (200), (220), (311), and (222), With the interplanar spacing 'd' was 2.41, 2.08, 1.476, 1.26 and  $1.20\text{ \AA}$  respectively. The cell parameter is  $a = 4.1800$ ,  $b = 4.1800$  and  $c = 4.1800$  with an average crystallite size was 25.075 nm.

XRD of Lithium doped NiO Nanoparticles has observed the crystalline phase identified a cubic structure and the peaks were matched with JCPDS card number ICSD 00-022-1189. At the crystalline phase all diffraction peaks at (111), (200), (220), (311), and (222) at an angle  $37.26^\circ$ ,  $43.3^\circ$ ,  $62.9^\circ$ ,  $75.43^\circ$  and  $79.43^\circ$ , with the interplanar spacing 'd' was 2.41, 2.09, 1.48, 1.26 and  $1.20\text{ \AA}$  respectively. At  $31.68^\circ$  and  $45.31^\circ$  with the plane (111) and (200) are lithium peaks. The lattice parameter is  $a = 4.1816$ ,  $b = 4.1816$ ,  $c = 4.1816$  with the crystallite size of 31.31 nm. XRD of Magnesium doped NiO Nanoparticles has

observed the crystalline phase identified a rhombohedral structure and the peaks were matched with JCPDS card number ICSD 00-044-1159. The average particles size was calculated at 27.48 nm. The crystalline phase all diffraction peaks at (101), (012), (110), (113), and (202) at an angle 37.26°, 43.3°, 62.9°, 75.43° and 79.430, with the 2.41, 2.08, 1.47, 1.25 and 1.20 Å respectively. At 28.36° and 40.55° with the planes (111) and (200) are magnesium peaks. The lattice parameter are a= 4.1790, b=4.1790, c=4.1790.

XRD of lithium and magnesium co-doped NiO nanoparticles was observed that the crystalline phase identified a rhombohedral structure and the peaks were matched with JCPDS card number ICSD 00-022-1189. The

average crystalline size was calculated at 24.06 nm. The crystalline phase all diffraction peaks at (111), (200), and (220) at an angle 37.26°, 43.3° and 62.9° with the more interplanar spacing d was 2.41, 2.08, 1.57, 1.47, and 1.26 Å respectively. At 28.45° and 40.82° with the planes (111) and (202) are lithium peaks, at 31.83° with the plane was (110). The lattice parameter are a= 4.1760, b=4.1760, c=4.1760.

The extra small peaks and peak shift in a graph show that the samples were doped and desired materials were achieved. The doped materials atoms are stayed at substitution and decrease the size of the material. All the XRD graphs are shown in Figure 1 (a-d).

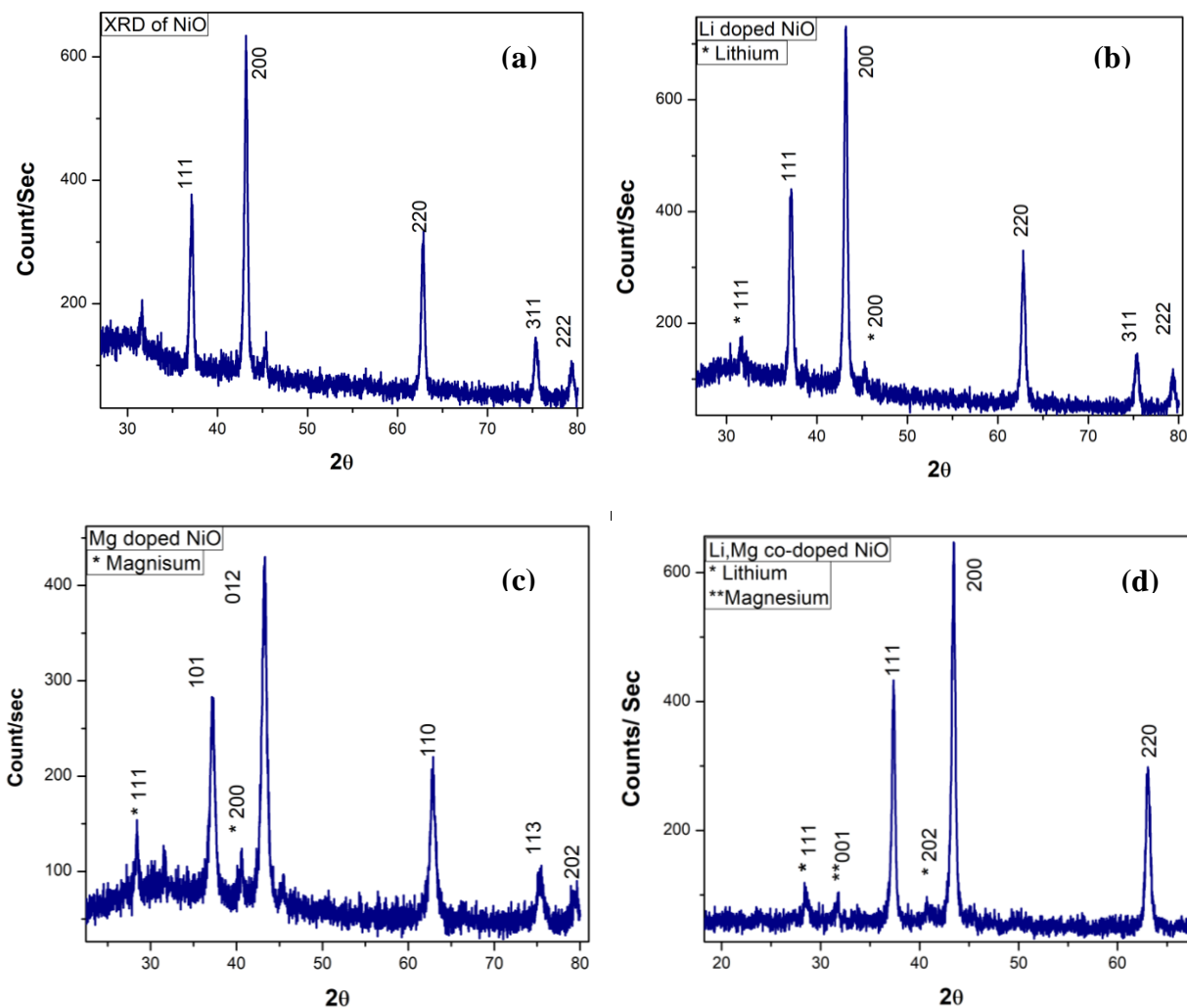


Figure 1: XRD pattern of (a) Pure, (b) Lithium Doped, (c) Magnesium, Lithium, and (d) Co-doped of Lithium and Magnesium with Nickel Oxide Nanoparticles.

### UV-Visible of Nickel Oxide Thin Film

Absorbance and Band Gap of ITO/NiO/CsPbI<sub>2</sub>Br, ITO/Li, NiO/CsPbI<sub>2</sub>Br, ITO/Mg, NiO/CsPbI<sub>2</sub>Br, ITO/Li, Mg, NiO/CsPbI<sub>2</sub>Br thin film was measured by using the absorbance formula, and Kubelka-Munk function respectively and draws the graph on origin software. All the Pure, Lithium, magnesium, and co-doped with

nickel oxide thin film showed a visible range of absorbance. The doped material has maximum absorbance and shows extra peaks due to the doping of the material and has an extra transition band. The bandgap of the pure materials has a direct bandgap with 3.09 eV. The doped materials have decreased the bandgap due to the transition states of the bandgap with 2.56 eV as shown in Figure 2 (a-d).

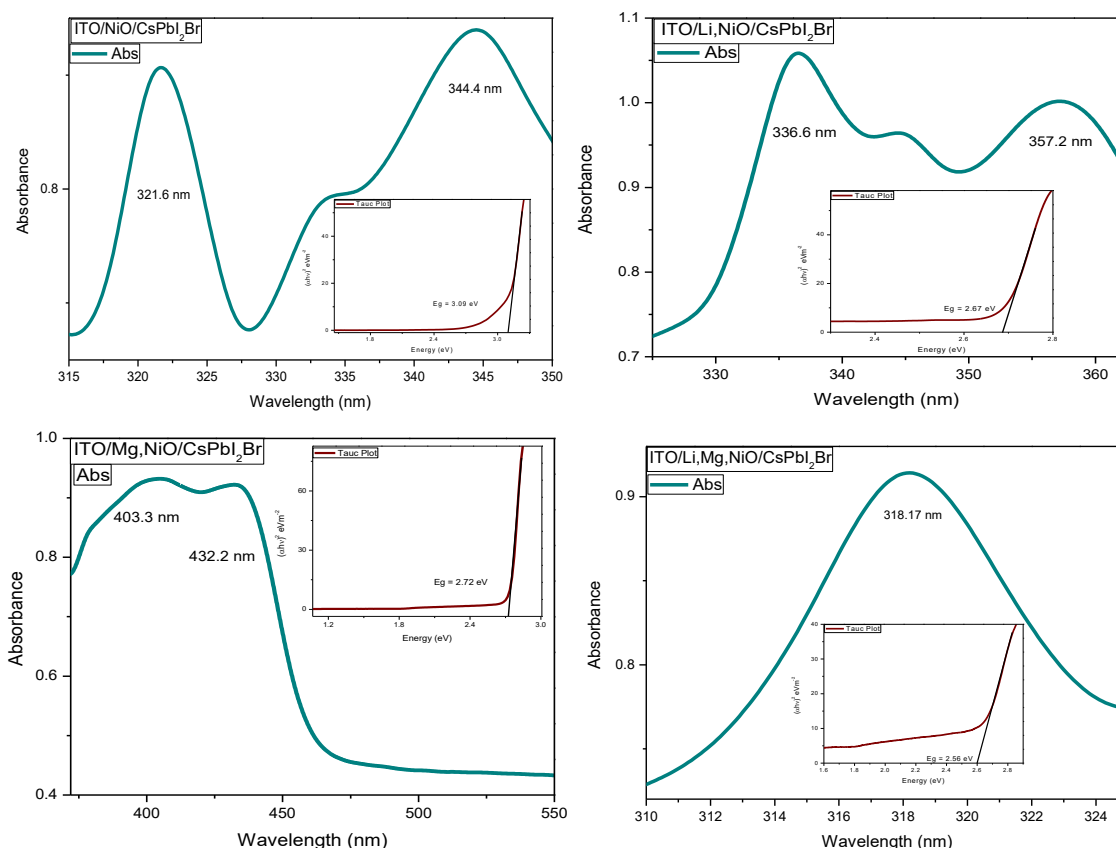


Figure 2: Absorbance and Band Gap of (a) ITO/NiO/CsPbI<sub>2</sub>Br, (b) ITO/Li, NiO/CsPbI<sub>2</sub>Br, (c) ITO/Mg, NiO/CsPbI<sub>2</sub>Br, (d) ITO/Li, Mg, NiO/CsPbI<sub>2</sub>Br Thin Film

### Rutherford Backscattering Spectroscopy (RBS)

Complementary compositional analyses of the thin films and the bare substrate were carried out using Rutherford Backscattering Spectroscopy. The given data draw the graph between normalized yield, Energy in MeV, and channel. The RBS shows the chemical

composition and thickness of the thin film. The RBS of ITO/Li, NiO ITO/NiO/CsPbI<sub>2</sub>Br, ITO/Mg, NiO, ITO/Li, NiO/CsPbI<sub>2</sub>Br, ITO/Mg, NiO/CsPbI<sub>2</sub>Br, ITO/Li, Mg, NiO/CsPbI<sub>2</sub>Br thin film are shown in Figure 3 (a-f).

In pure NiO thin film, the peak of Nickel and bromine near the 1500 channel at 1.5 MeV energy. The strongest peak of carbon and

oxygen showed near the 500 channels at 0.5 MeV. The carbon peak on the thin film is due to the large impurity of carbon. The RBS of CsPbI<sub>2</sub>Br thin film deposited on Nickel Oxide

thin film and ITO glass substrate. The peak of iodine at 1620 channel with the 1.6 MeV energy. The peak of lead at 1750 channel with the 1.8 MeV.

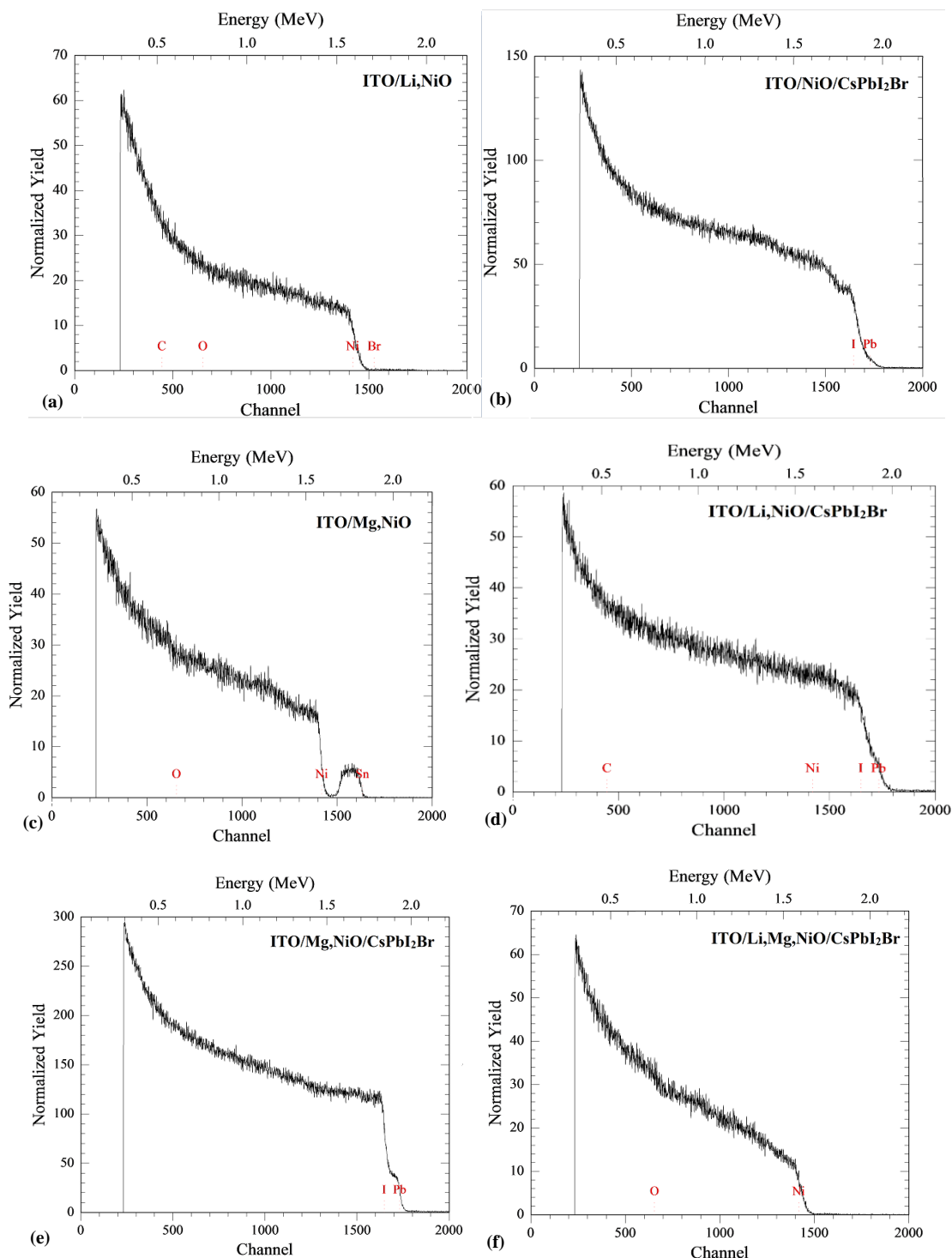


**Figure 3: RBS of (a) ITO/Li,NiO (b) ITO/NiO/CsPbI<sub>2</sub>Br, (c) ITO/Mg,NiO, (d) ITO/Li, NiO/CsPbI<sub>2</sub>Br (e) ITO/Mg, NiO/CsPbI<sub>2</sub>Br, (f) ITO/Li, Mg, NiO/CsPbI<sub>2</sub>Br Thin Film**

The RBS of Magnesium doped with Nickel Oxide thin film deposited on ITO glass substrate. The peak of Nickel at 1450 channel with the 1.5 MeV energy and the peak of tin at 1650 channel with 1.7 MeV energy. The peak of oxygen was at 550 channels with 0.7 eV. The RBS of CsPbI<sub>2</sub>Br thin film deposited on Lithium doped with Nickel Oxide thin film and ITO glass substrate. The peak of Nickel at 1430 channel with the 1.5 MeV energy. The peak of lead and Iodine near the 1650 and 1750 channel with 1.75 and 1.8 MeV energy. The peak of carbon was at 450 channels with 0.45 eV energy. The RBS of CsPbI<sub>2</sub>Br thin film deposited on Magnesium doped with Nickel Oxide thin film and ITO glass substrate. The peak of Iodine near the 1650 channel with 1.75 MeV energy. The peak of lead at 1700 with the 1.8 MeV energy. The RBS of CsPbI<sub>2</sub>Br thin film deposited on Lithium and Magnesium doped with Nickel Oxide thin film and ITO glass substrate. The peak of Nickel at 1490 channel with the 1.4 MeV energy. The peak of oxygen at 650

channels with 0.7 MeV. The peaks are shown in Figure 3 (a-f) (Atak, et al., 2020)

### IV Measurement

IV measurement by using a solar simulator with the 1000  $\text{wm}^{-2}$  intensity of light, under the condition of dark and light. The given data from the simulator draw the graph between current and voltage. The fill factor FF and power conversion efficiency PCE was measured by using a formula. Lithium and Magnesium doped with Nickel Oxide thin film deposited on ITO, then deposited perovskite layer. After that measure the IV curve under the dark and light conditions. In dark conditions, the value of slope was 2.8. The identity factor was measured at 13.96. Under the light condition, all the materials showed different efficiency and fill factors. The minimum values were due to impurity and non-uniform thickness of the layer of the thin film. As the graphs show in Figures 5 to 11. All the calculated values of power conversion efficiency and fill factor are shown in table 1 (Hadi et al., 2020).

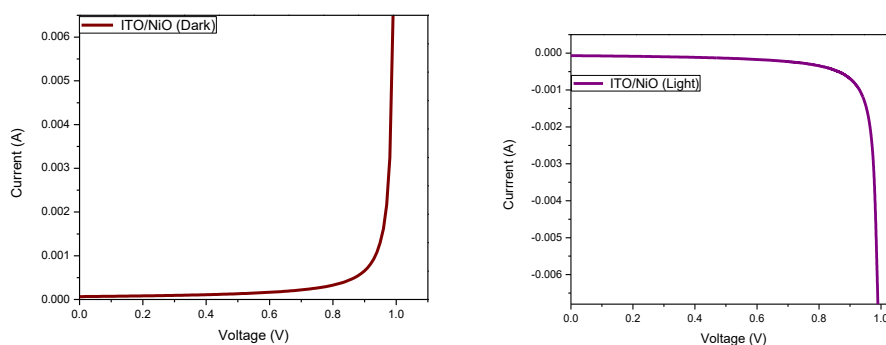


Figure 4: IV Curve of ITO/NiO Thin Film Layers under Dark and Light Condition

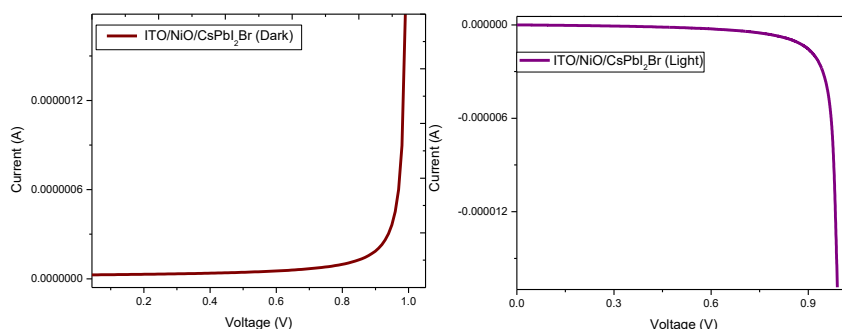
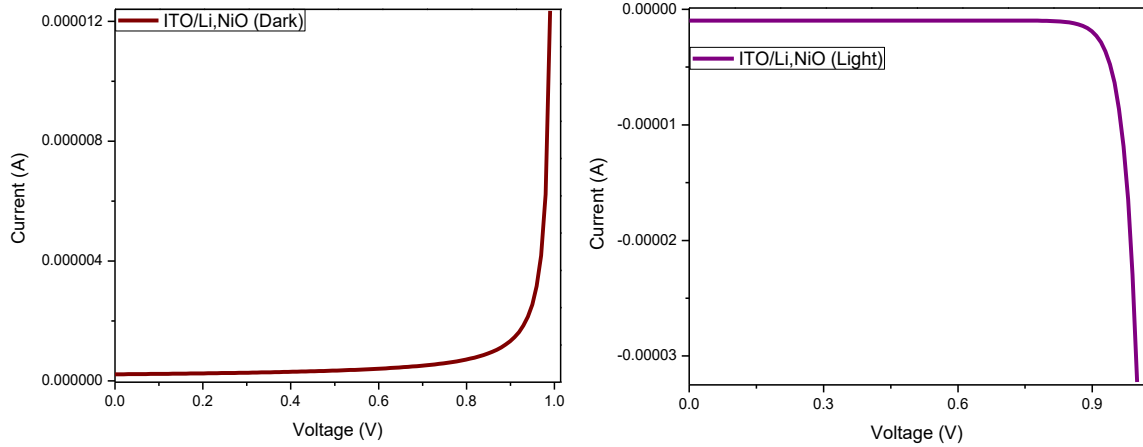
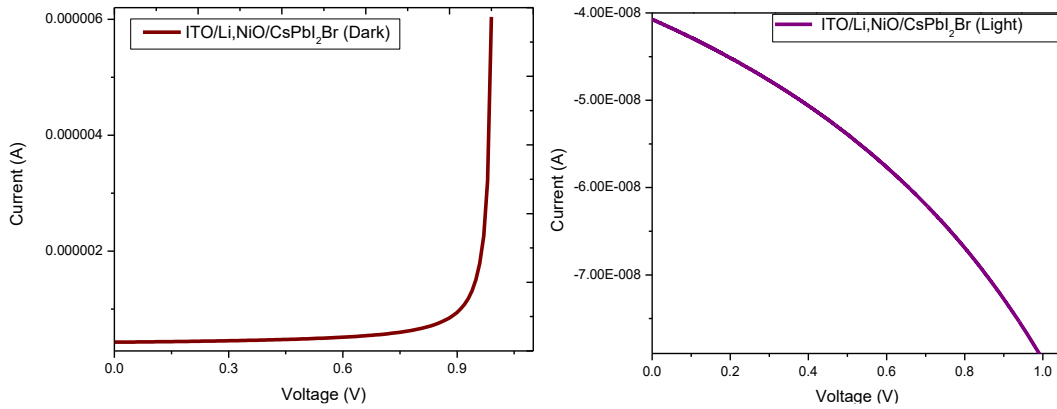


Figure 5: IV Curve of ITO/NiO/CsPbI<sub>2</sub>Br Thin-Film Layers under the Dark and Light Condition



**Figure 6: IV Curve of ITO/Li, NiO Thin Film Layers under Dark and Light Condition**



**Figure 7: IV Curve of ITO/Li, NiO/CsPbI<sub>2</sub>Br Thin-Film Layers under the Dark and Light Conditions**

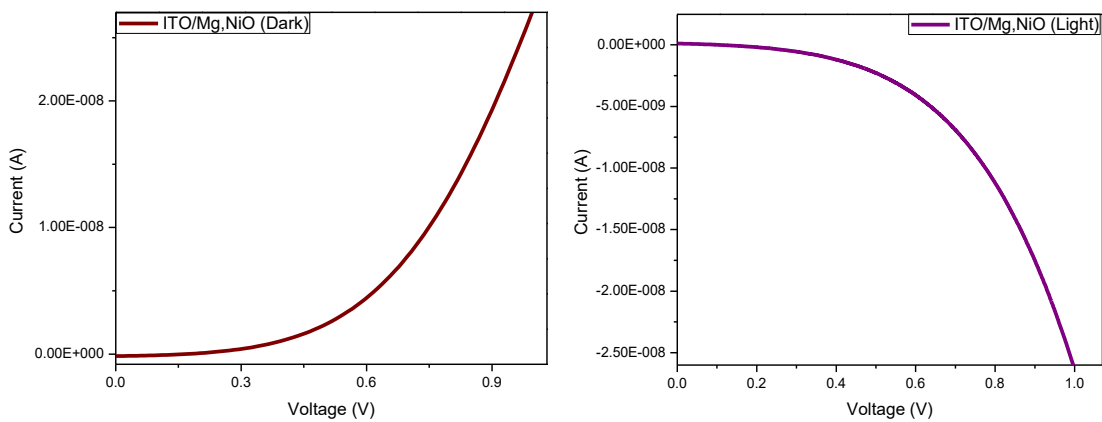


**Figure 8: IV Curve of ITO/Mg, NiO Thin Film Layers under Dark and Light Condition**

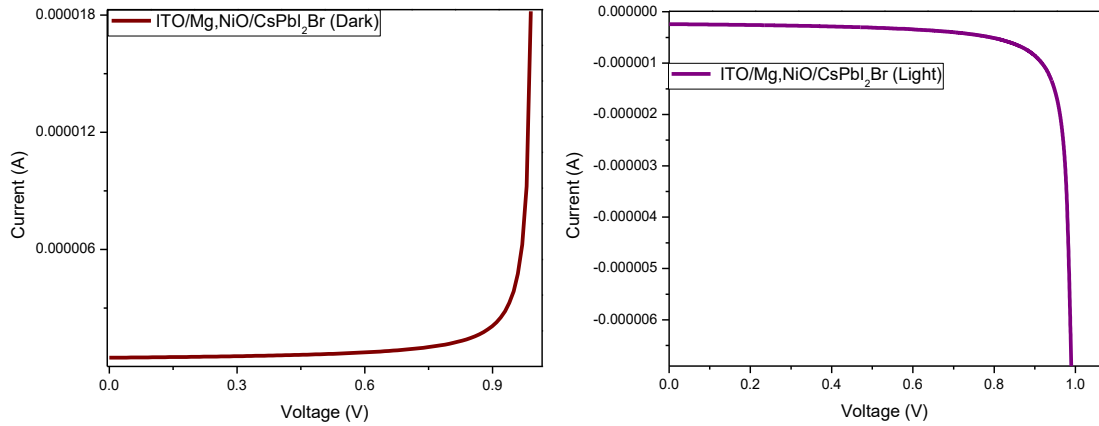


**Figure 9: IV Curve of ITO/Mg, NiO/CsPbI<sub>2</sub>Br Thin Films Layers under the Dark and Light Condition**

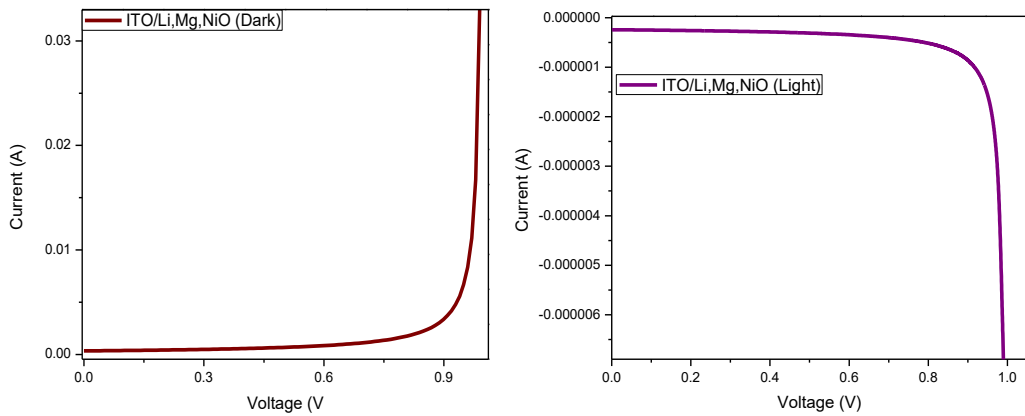


**Figure 10: IV Curve of ITO/Li, Mg, NiO Thin Films Layers under Dark and Light Condition**

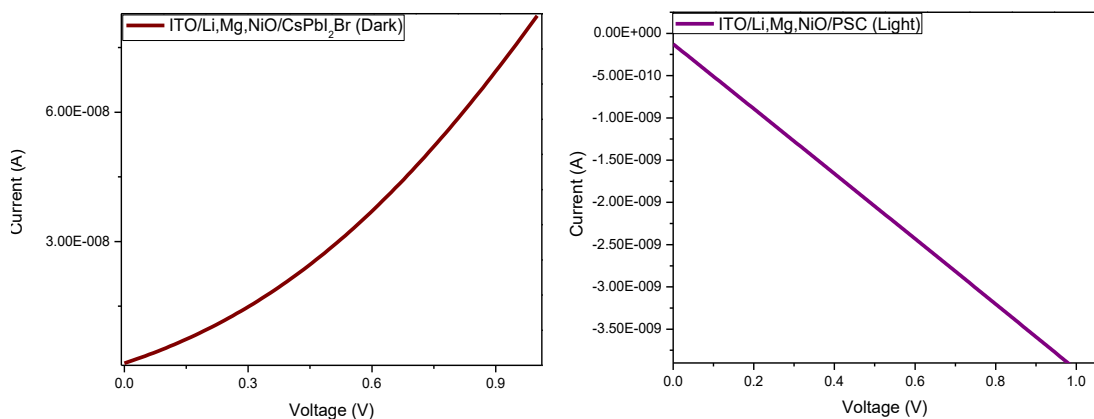


**Figure 11: IV Curve of ITO/Li, Mg, NiO/CsPbI<sub>2</sub>Br Thin-Film Layers under Dark and Light Condition**

**Table 4.1: Calculations of Power Conversion Efficiency for Inorganic Perovskite Solar Cell.**

Sr.No	Materials	V <sub>oc</sub>	I <sub>sc</sub>	V <sub>mp</sub>	I <sub>mp</sub>	FF	% PCE
01	ITO/NiO	9.2	9.1	6.3	7.1	0.52	4.3
02	ITO/NiO/CsPbI <sub>2</sub> Br	9.3	9.6	8.6	8.5	0.81	7.2
03	ITO/Li, NiO	9.4	9.6	8.5	8.8	0.82	7.3
04	ITO/Li, NiO/CsPbI <sub>2</sub> Br	9.1	9.2	5.1	5.2	0.30	2.4
05	ITO/Mg, NiO	9.4	9.8	5.3	5.8	0.33	3.01
06	ITO/Mg, NiO/CsPbI <sub>2</sub> Br	9.3	9.9	8.9	8.6	0.82	7.64
07	ITO/Li, Mg, NiO	9.5	8.6	8.7	8.8	0.83	7.65
08	ITO/Li, Mg, NiO/CsPbI <sub>2</sub> Br	9.2	8.5	7.4	7.95	0.70	5.5

### CONCLUSION

We have successfully synthesized nickel oxide nanoparticles with lithium and magnesium co-doped as hole transport layer by co-precipitation method and perovskite layer was prepared by co-precipitation method. The thin film of nickel oxide was prepared by making the paste and deposited on ITO glass by doctor blade process. After that perovskite layer is an absorber layer deposited on nickel oxide thin film and characterize to confirm the properties of the thin film.

XRD confirmed the crystallinity and phases of the materials with an average crystal size was 24 nm. UV visb and DRS confirmed the optical properties by finding the absorbance and bandgap of the materials. The bandgap of the material was varied by adding the doping from 3.74 eV to 3.40 eV with the absorbance to near the visible range. The bandgap of ITO/Li, Mg, NiO/CsPbI<sub>2</sub>Br was 2.56 eV. RBS confirmed the chemical composition of the thin film. It showed the thickness of the thin film was good. IV curve measurement confirmed the conductivity and efficiency of the materials under dark and light conditions. It confirmed that the efficiency of pure nickel oxide thin film was 4.3 %, Lithium and Magnesium co-doped with nickel oxide thin film with the perovskite layer was the highest

efficiency 7.65 % with the 83 % fill factor FF. The efficiency of the material was very low due to the addition of impurities from the surrounding and non-uniform thickness layer of the material.

### REFERENCES

- Atak, G., Pehlivan, İ. B., Montero, J., Primetzhofer, D., Granqvist, C. G., & Niklasson, G. A. (2020). Electrochromism of nitrogen-doped tungsten oxide thin films. *Materials Today: Proceedings*, 33, 2434-2439.
- Beal, R. E., Slotcavage, D. J., Leijtens, T., Bowring, A. R., Belisle, R. A., Nguyen, W. H., & McGehee, M. D. (2016). Cesium lead halide perovskites with improved stability for tandem solar cells. *The journal of physical chemistry letters*, 7(5), 746-751.
- Chen, W., Chen, H., Xu, G., Xue, R., Wang, S., Li, Y., & Li, Y. (2019). Precise Control of Crystal Growth for Highly Efficient CsPbI<sub>2</sub>Br Perovskite Solar Cells. *Joule*, 3(1), 191-204.
- Duan, J., Hu, T., Zhao, Y., He, B., & Tang, Q. (2018). Carbon-Electrode-Tailored All Inorganic Perovskite Solar Cells To Harvest Solar and Water-Vapor Energy. *Angewandte Chemie International Edition*, 57(20), 5746-5749.

- Duan, J., Zhao, Y., Yang, X., Wang, Y., He, B., & Tang, Q. (2018). Lanthanide Ions Doped CsPbBr<sub>3</sub> Halides for HTM-Free 10.14%-Efficiency Inorganic Perovskite Solar Cell with an Ultrahigh Open-Circuit Voltage of 1.594 V. *Advanced Energy Materials*, 8(31), 1802346.
- Frolova, L. A., Anokhin, D. V., Piryazev, A. A., Luchkin, S. Y., Dremova, N. N., Stevenson, K. J., & Troshin, P. A. (2016). Highly efficient all-inorganic planar heterojunction perovskite solar cells produced by thermal coevaporation of CsI and PbI<sub>2</sub>. *The journal of physical chemistry letters*, 8(1), 67-72.
- Fu, Y., Zhu, H., Chen, J., Hautzinger, M. P., Zhu, X. Y., & Jin, S. (2019). Metal halide perovskite nanostructures for optoelectronic applications and the study of physical properties. *Nature Reviews Materials*, 4(3), 169-188.
- Hadi, A. A., Badr, B. A., Mahdi, R. O., & Khashan, K. S. (2020). Rapid laser fabrication of Nickel oxide nanoparticles for UV detector. *Optik*, 219, 165019.
- He, J., Xiang, Y., Zhang, F., Lian, J., Hu, R., Zeng, P., & Qu, J. (2018). Improvement of red light harvesting ability and open circuit voltage of Cu: NiOx based pin planar perovskite solar cells boosted by cysteine enhanced interface contact. *Nano Energy*, 45, 471-479.
- Irwin, M. D., Buchholz, D. B., Hains, A. W., Chang, R. P., & Marks, T. J. (2008). p-Type semiconducting nickel oxide as an efficiency-enhancing anode interfacial layer in polymer bulk-heterojunction solar cells. *Proceedings of the National Academy of Sciences*, 105(8), 2783-2787.
- Lei, J., Gao, F., Wang, H., Li, J., Jiang, J., Wu, X., ... & Liu, S. F. (2018). Efficient planar CsPbBr<sub>3</sub> perovskite solar cells by dual-source vacuum evaporation. *Solar Energy Materials and Solar Cells*, 187, 1-8.
- Liang, J., Zhao, P., Wang, C., Wang, Y., Hu, Y., Zhu, G., & Jin, Z. (2017). CsPb<sub>0.9</sub>Sn<sub>0.1</sub>Br<sub>2</sub> based all-inorganic perovskite solar cells with exceptional efficiency and stability. *Journal of the American Chemical Society*, 139(40), 14009-14012.
- Liao, G., Duan, J., Zhao, Y., & Tang, Q. (2018). Toward fast charge extraction in all inorganic CsPbBr<sub>3</sub> perovskite solar cells by setting intermediate energy levels. *Solar Energy*, 171, 279285.
- Mali, S. S., Kim, H., Kim, H. H., Shim, S. E., & Hong, C. K. (2018). Nanoporous p type NiOx electrode for pin inverted perovskite solar cell toward air stability. *Materials Today*, 21(5), 483-500.
- Mali, S. S., Kim, H., Kim, H. H., Shim, S. E., & Hong, C. K. (2018). Nanoporous p-type NiOx electrode for pin inverted perovskite solar cell toward air stability. *Materials Today*, 21(5), 483-500.
- Chen, W., Xu, L., Feng, X., Jie, J., & He, Z. (2017). Metal acetylacetonate series in interface engineering for full low-temperature-processed, high-performance, and stable planar perovskite solar cells with conversion efficiency over 16% on 1 cm<sup>2</sup> scale. *Advanced Materials*, 29(16), 1603923.
- Murugadoss, G., & Thangamuthu, R. (2019). Metals doped cesium based all inorganic perovskite solar cells: Investigations on Structural, morphological and optical properties. *Solar Energy*, 179, 151-163.
- Ouyang, D., Huang, Z., & Choy, W. C. (2019). Solution-processed metal oxide nanocrystals as carrier transport layers in organic and perovskite solar cells. *Advanced Functional Materials*, 29(1), 1804660.

- Pei, Y., Guo, H., Hu, Z., Zhang, J., & Zhu, Y. (2020). BiBr<sub>3</sub> as an additive in CsPbBr<sub>3</sub> for carbon-based all-inorganic perovskite solar cell. *Journal of Alloys and Compounds*, 835, 155283.
- Qin, P., He, Q., Ouyang, D., Fang, G., Choy, W. C., & Li, G. (2017). Transition metal oxides as hole-transporting materials in organic semiconductor and hybrid perovskite based solar cells. *Science China Chemistry*, 60(4), 472-489.
- Sanchez, S., Christoph, N., Grobety, B., Phung, N., Steiner, U., Saliba, M., & Abate, A. (2018). Efficient and Stable Inorganic Perovskite Solar Cells Manufactured by Pulsed Flash Infrared Annealing. *Advanced Energy Materials*, 8(30), 1802060.
- Sun, J., Lu, J., Li, B., Jiang, L., Chesman, A. S., Scully, A. D., & Jasieniak, J. J. (2018). Inverted perovskite solar cells with high fill-factors featuring chemical bath deposited mesoporous NiO hole transporting layers. *Nano energy*, 49, 163-171.
- Sun, J., Lu, J., Li, B., Jiang, L., Chesman, A. S., Scully, A. D., ... & Jasieniak, J. J. (2018). Inverted perovskite solar cells with high fill-factors featuring chemical bath deposited mesoporous NiO hole transporting layers. *Nano Energy*, 49, 163-171.
- Sveinbjörnsson, K., Thein, N. K. K., Saki, Z., Svanström, S., Yang, W., Cappel, U.B & Johansson, E. M. (2018). Preparation of mixed-ion and inorganic perovskite films using water and isopropanol as solvents for solar cell applications. *Sustainable Energy & Fuels*, 2(3), 606-615.
- Tang, K. C., You, P., & Yan, F. (2018). Highly Stable All-Inorganic Perovskite Solar Cells Processed at Low Temperature. *Solar RRL*, 2(8), 1800075.
- Thambidurai, S., Gowthaman, P., Venkatachalam, M., & Suresh, S. (2020). Enhanced bactericidal performance of nickel oxide-zinc oxide nanocomposites synthesized by facile chemical co-precipitation method. *Journal of Alloys and Compounds*, 830, 154642.
- Wang, P., Zhang, X., Zhou, Y., Jiang, Q., Ye, Q., Chu, Z., ... & You, J. (2018). Solvent controlled growth of inorganic perovskite films in dry environment for efficient and stable solar cells. *Nature communications*, 9(1), 2225.
- Xiang, He, J., Y., Zhang, F., Lian, J., Hu, R., Zeng, P., ... & Qu, J. (2018). Improvement of red light harvesting ability and open circuit voltage of Cu: NiO<sub>x</sub> based pin planar perovskite solar cells boosted by cysteine enhanced interface contact. *Nano Energy*, 45, 471-479.
- Zhang, H., Cheng, J., Lin, F., He, H., Mao, J., Wong, K. S., ... & Choy, W. C. (2015). Pinhole free and surface-nanostructured NiO<sub>x</sub> film by room-temperature solution process for high-performance flexible perovskite solar cells with good stability and reproducibility. *ACS nano*, 10(1), 1503-1511.
- Zhang, H., Cheng, J., Lin, F., He, H., Mao, J., Wong, K. S., ... & Choy, W. C. (2016). Pinhole-free and surface-nanostructured NiO<sub>x</sub> film by room-temperature solution process for high-performance flexible perovskite solar cells with good stability and reproducibility. *ACS nano*, 10(1), 1503-1511.
- Zhang, S., Wu, S., Chen, W., Zhu, H., Xiong, Z., Yang, Z., & Chen, W. (2018). Solvent engineering for efficient inverted perovskite solar cells based on inorganic CsPbI<sub>2</sub>Br light absorber. *Materials today energy*, 8, 125-133.
- Zhang, Y., Zhang, Z., Liu, Y., Liu, Y., Gao, H., & Mao, Y. (2019). An inorganic hole transport material of CuInSe<sub>2</sub> for stable and efficient perovskite solar cells. *Organic Electronics*.